Journal of Materials Chemistry

Cite this: J. Mater. Chem., 2012, 22, 11529

www.rsc.org/materials

PAPER

PAMAM-functionalized water soluble quantum dots for cancer cell targeting

Mehriban Akin,[a] Rebecca Bongartz,[b] Johanna G. Walter,[b] Dilek Odaci Demirkol,[a] Frank Stahl,*[b] Suna Timur*[a] and Thomas Scheper[b]

Received 19th February 2012, Accepted 12th April 2012
DOI: 10.1039/c2jm31030a

Herein, the phase-transfer reaction of quantum dots (QDs) with amine-terminated polyamidoamine (PAMAM) dendrimers with controllable ligand molar ratios was achieved. The unique properties of PAMAM allowed us to build up structurally and electrostatically stabilized water soluble QD complexes. Synthesized conjugates were characterized in terms of fluorescence and UV-Vis profiles, hydrodynamic size, number of surface dendrimer groups, and stability. Cytotoxic effects of conjugates for MCF-7, A-549 and HEP-G2 cancer cells were assessed based on cell viability using MTT assay. Cytotoxicity results were expressed as no observable adverse effect concentration (NOAEC), 50% inhibitory concentration (IC_{50}) and total lethal concentration (TLC) values (μM). Furthermore, HER2 receptor-mediated targeting efficiency of antibody labelled P/QDs conjugates was evaluated by successful staining of MCF-7 cells with bioconjugates. Uniquely, effective cell internalization was achieved with well-characterized antibody coupled P/QDs in contrast to antibody free P/QDs conjugates. Fluorescence microscopy images demonstrated that the designed PAMAM-derivatized QDs nanoparticles show great potential in the areas of cellular imaging and targeted therapy.

Introduction

In the last decade semiconductor nanocrystals (so-called quantum dots, QDs) have been introduced as a new type of biolabelling agent. QDs have unique optical properties in comparison to organic fluorophores, such as broad absorption spectra, narrow emission in combination with broad-band excitation allowing multi-color labelling of different compartments/structures/processes simultaneously, reduced tendency to photobleaching, and long fluorescence lifetime.[1] Also QDs have large surface areas to interact with therapeutic and diagnostic agents which makes QDs ideal for multifunctional imaging agents.[2] Many articles[3–12] and reviews[13–18] deal with biological applications of colloidal QDs. As fluorescent markers, QDs are commonly used to visualize cellular structures, certain compounds inside the cells to investigate cellular processes, and label tumor cells. Since it was proved that quantum dots are incorporated by living cells,[19] the uptake of those nanocrystals into cells became important in applications such as gene, drug, and nucleic acid delivery.[20]

The synthesis of highly fluorescent quantum dots (QDs) is generally performed in organic solvents such as trioctylphosphine oxide (TOPO) and hexadecylamine (HDA) at high temperature (>200 °C).[21] The resulting monodisperse QDs are coated with hydrophobic organic compounds. Thus they form sterically stabilized colloids in non-polar solvents and coagulate in polar solvents. For biosensing applications, QDs have to be conjugated to biological molecules. This necessitates transfer of QDs into aqueous solutions which is quite challenging. In order to mediate water solubility, the surfactant layer of the QDs should be replaced or coated with another layer introducing electrostatic charge or hydrophilic head groups, which trigger water solubility. It is crucial to determine a reliable surface processing chemistry for QDs. Highly branched dendritic macromolecules such as polyamidoamine (PAMAM) provide a unique surface of multiple chains terminated with functional groups for synthetic approaches. Their multiple conjugation sites provide densely functionalized and structurally stable architectures.[22] PAMAM with variable terminal groups can be effectively applied to modify QDs surfaces. However, amine-terminated dendrimers exhibit some advantages which are electrostatic stabilization of QDs by their polyelectrolyte nature, high cell association capability, improved membrane permeation ability (especially those of higher generation),[23,24] and high buffering capacity that promotes endosomal escape. Ingested QDs are not accessible to cytosol so they are stored in vesicles. By virtue of the strong buffering capacity of primary and tertiary amines, PAMAM can mediate escape from internal vesicles.[25–28] On the other hand, this endosomal escape process will prevent quantum dots losing their fluorescence under acidic conditions in vesicles.[29]

So far there are at least four intensively identified nanotechnology platforms that represent precise nanostructures: I)

[a]Ege University, Faculty of Science, Biochemistry Department, 35100 Bornova-Izmir, Turkey. E-mail: suna.timur@ege.edu.tr; Fax: +90 232 3438634; Tel: +90 232 3438634
[b]Gottfried Wilhelm Leibniz University of Hannover, Institute for Technical Chemistry, Callinstr. 5, 30167 Hannover, Germany. E-mail: stahl@iftc.uni-hannover.de; Fax: +49 511 7623004; Tel: +49 511 7622968

nanotubes, II) fullerenes, III) quantum dots and IV) dendrons/dendrimers.[30] In our work, we combined the above mentioned advantageous characteristics of PAMAM dendrimers with effective fluorescence properties of CdSe/ZnS QDs in order to design well characterized water soluble QD conjugates. To the best of our knowledge, the use of PAMAM dendrimers to modify QDs for biological applications is very recent.[27,30] Mostly thiol-terminated dendrons/dendrimers were utilized to encapsulate nanocrystals.[30–33] Since thiol groups are very active to photooxidation,[32] other functional moieties such as amine, hydroxyl, carboxylic acid, phosphine oxide, and phosphonic oxide are under consideration. Recently, Zhao *et al.* (2010) synthesized folate-poly(ethylene glycol)-PAMAM functionalized QDs to evaluate cellular uptake by HeLa cells. That study is the only one to date that modifies QDs surface with amine-terminated dendrimer ligands.[34]

Herein, water solubilization of QDs *via* amine-terminated PAMAM dendrimers with controllable ligand densities was successfully achieved. Afterwards, the effects of surface charge and density of the PAMAM ligands on cellular targeting were examined. In order to investigate the application of the designed PAMAM/QDs conjugates, the conjugates were coupled to HER2 antibodies to label MCF-7 human breast cancer cells through HER2 receptor-mediated endocytosis. The cellular uptake of antibody coupled PAMAM/QDs was examined under fluorescence microscopy.

Results

Characterization studies

PAMAM generation 5 (P-G5) dendrimers with amine surface groups were used as a coating agent for HDA capped QDs. After the mixture of QD nanocrystals and PAMAM solution was incubated for 15 h, PAMAM/QD complexes were precipitated with ethyl acetate. The supernatant was discarded and the precipitant was dissolved in PBS buffer. Clearly, QDs were transferred to the polar phase at the end of the procedure. Amine groups of the original surface ligands (HDA) were replaced with the amine groups of PAMAM during the reaction. Fig. 1 outlines the direct ligand-exchange reactions between PAMAM dendrimer ligands and HDA-stabilized CdSe/ZnS core-shell QDs (HDA-QDs).

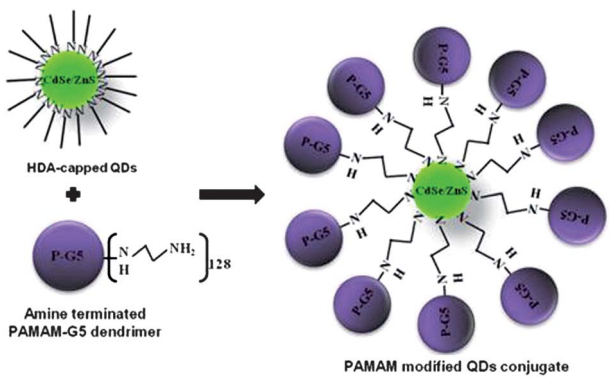

Fig. 1 Ligand exchange reaction between HDA-stabilized QDs and PAMAM-G5 dendrimers. Terminal amine groups of HDA were replaced with terminal amine groups of PAMAM. Resulting PAMAM-modified QDs complexes (P/QDs) were dissolved in PBS buffer pH 7.4.

The effect of conjugation on fluorescence characteristics of the QDs was examined *via* fluorescence spectroscopy. The fluorescence spectrum of PAMAM-derivatized QDs shows that there isn't any significant shift of the maximum emission peak in comparison with free QDs at 563 nm (Fig. 2A). This result indicates that despite water solubilization of QDs, fluorescent properties of QDs don't exhibit any major changes. UV-vis spectra of free QDs and PAMAM molecules have absorbance maxima at 545 nm and 280 nm respectively (Fig. 2B). Contrasting those with the UV-vis profiles of PAMAM-attached QDs, the same peaks at 280 nm for PAMAM and 545 nm for QDs demonstrate successful coupling of PAMAM to the QDs. Additionally, coupling of antibodies doesn't result in any changes in the optical properties of QDs either.

Further, QDs were modified with different amounts of PAMAM and Bradford assay was used to estimate the numbers of PAMAM molecules coupled to the QDs. The Bradford assay is based on an absorbance shift of the dye Coomassie Brilliant Blue G-250.[35] Under acidic conditions the reddish form of the dye is converted into its bluer form to bind to the molecule being assayed. The formation of the complex between dye and molecule is caused by the ionic interactions between the negative charge of the dye and positive charges of primary and tertiary

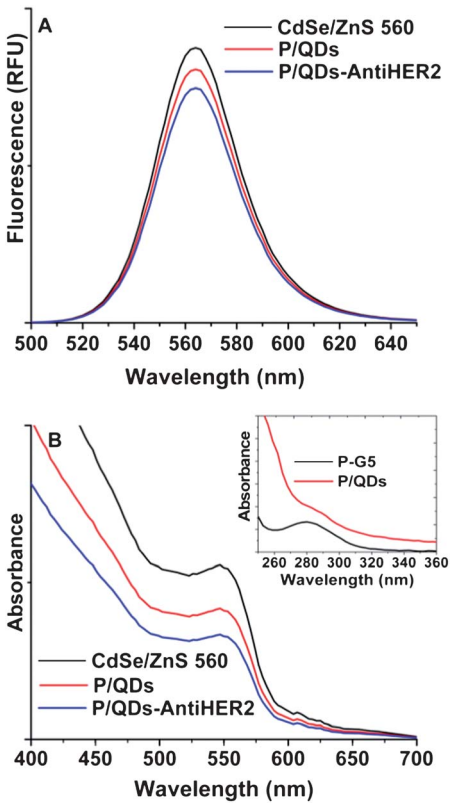

Fig. 2 Fluorescence (A) and, UV-vis (B) spectra of unmodified QDs, PAMAM-modified QDs, and HER2 specific antibody-coupled P/QDs conjugates. (A) Surface modification process didn't cause any major changes in fluorescence properties of QDs. Insert shows specific peaks at 280 nm for PAMAM and 545 nm for QDs at P/QDs conjugates proving a successful ligand-exchange reaction.

amine groups of PAMAM. The bound form of the dye has an absorption maximum at 595 nm. Accordingly, by using calibration curve for PAMAM with a linear range 0.1 μM–2.5 μM ($y = 0.994x - 0.005$; $R^2 = 0.999$), it was calculated that a maximum of 28 PAMAM molecules were coupled to QD. Fig. 3 gives estimated numbers of PAMAM bound to the QD surface and their corresponding fluorescence intensities. The fluorescence of P/QDs conjugates increases as a function of increasing number of PAMAM molecules until it reaches maximum binding point. The yield of the surface modification processes in terms of PAMAM coupling efficiency is 93.3% in the case of 30-fold molar excess of PAMAM involved in the reaction.

The hydrodynamic diameters of P/QDs conjugates were evaluated by using dynamic light scattering (DLS). Particle diameters of free PAMAM (P-G5), QDs modified with *ca.* 14 (P14/QDs), and *ca.* 28 (P28/QDs) PAMAM molecules are given in Fig. 4. According to the DLS results, the size of PAMAM G5 dendrimers was estimated to be 5.6 nm, which is consistent with the early reported size of Tomalia-type PAMAM G5 dendrimers with amine surface functionalities which is 5.7 nm.[22] While P14/QDs nanoparticles had narrow distributions around 32.7 nm, P28/QDs particles feature a wide distribution around 58.8 nm indicating relatively heterogeneous size distribution. Unmodified QDs in toluene have a size of approximately 3.7 nm. The increase in size of QDs is reasonable because surface coating with a layer of PAMAM increases the radius of nanocrystals due to the expanded hydrated layer. In addition to DLS, the size of P14/QDs conjugate was also evaluated with SEM. The size of the lyophilized form of P14/QDs was calculated to be 31.81 ± 3.40 nm. Even though hydrodynamic size doesn't indicate real size, DLS and SEM results for P14/QDs conjugates seem to be in good agreement. Reduced size of QD-based probes is essential to achieve better tumor targeting and cellular uptake.[36] Thus, P14/QDs conjugates were taken into consideration for further studies because of their relatively small size and homogeneous size distribution.

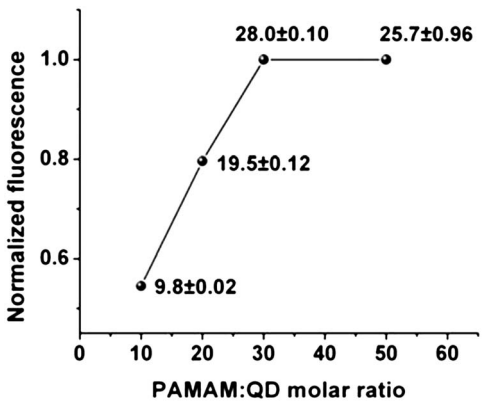

Fig. 3 Normalized fluorescence of QD nanoparticles modified with 10-, 20-, 30-, and 50-fold molar excess of PAMAM. Inset numbers indicate PAMAM molecules conjugated per QD calculated *via* Bradford assay. 9.8 ± 0.02, 19.5 ± 0.12, 28.0 ± 0.10, and 25.7 ± 0.96 PAMAM molecules were estimated to be conjugated per QD when QD nanocrystals were treated with 10-, 20-, 30-, and 50-fold excess of PAMAM molecules respectively. Briefly, a maximum of approximately 28 PAMAM molecules can cover a QD surface. Values are the mean ± standard deviation of the data ($N = 3$).

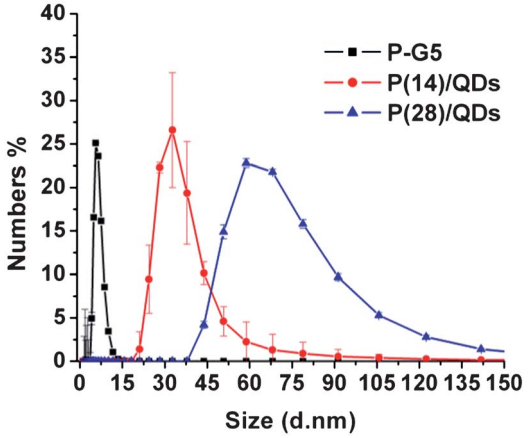

Fig. 4 Size distribution of PAMAM and PAMAM-modified QDs conjugates in aqueous solution. Results showed that PAMAM molecules have a hydrodynamic diameter of 5.61 ± 0.0003 (black line), while QDs modified with 14 PAMAM molecules (P14/QDs) have a hydrodynamic diameter of 32.67 ± 0.216 nm (red line), and P28/QDs particles have 58.77 ± 0.029 nm (blue line) hydrodynamic diameters. Values are the mean ± standard deviation of the data ($N = 3$).

Photostability

Enhanced photostability is of particular importance for long-term experiments, *e.g.* for time-resolved studies, such as fluorescence labelling of transport processes in cells, or tracking the path of single membrane-bound molecules.[37] A major advantage of using QDs instead of organic fluorophores for bioanalytical purposes is their increased photostability. QDs in chloroform or toluene do not show any photobleaching. In contrast, modified QDs undergo fast photooxidation when they are transferred to polar solvent *via* phase-transfer reactions. Polymer coatings seem to enable photooxidation at surface defects of the QDs.[38] When PAMAM-derivatized QDs were stored in the dark, they remained fluorescent for at least 4 weeks without any significant decrease in their fluorescence intensities (data not shown).

Evaluation of cytotoxicity

Dose dependent cytotoxicity effects of P/QDs were evaluated by using standard 3-(4,5-dimethylthiazol-2-yl)-2,5-diphenyl tetrazolium bromide (MTT) assays. Toxic effects of QDs don't only arise from nanocrystals themselves but also from surface covering molecules.[39,40] Cationic nanoparticles are often considered to be cytotoxic agents, due to their electrostatic interactions with negatively charged glycocalyx on cell membranes.[41] Thus it is essential to evaluate the toxicity effects of the PAMAM-coated QDs (P14/QDs) using the international standard test for *in vitro* cytotoxicity (ISO 10993-5) applying MTT for cell viability. Fig. 5 shows the cell viability data obtained from P14/QDs conjugates at different QDs concentrations. Despite the potentially toxic effects of PAMAM at concentrations higher than 5.0 μM,[42] QDs induce cell growth inhibition at even lower concentrations. In this study, MCF-7 and typical model cell lines A-549 and HEP-G2 were exposed to P14/QDs conjugates up to 0.5 μM QDs where concentration of conjugated PAMAM was 7.0 μM, for 4 h at 37 °C. Since native

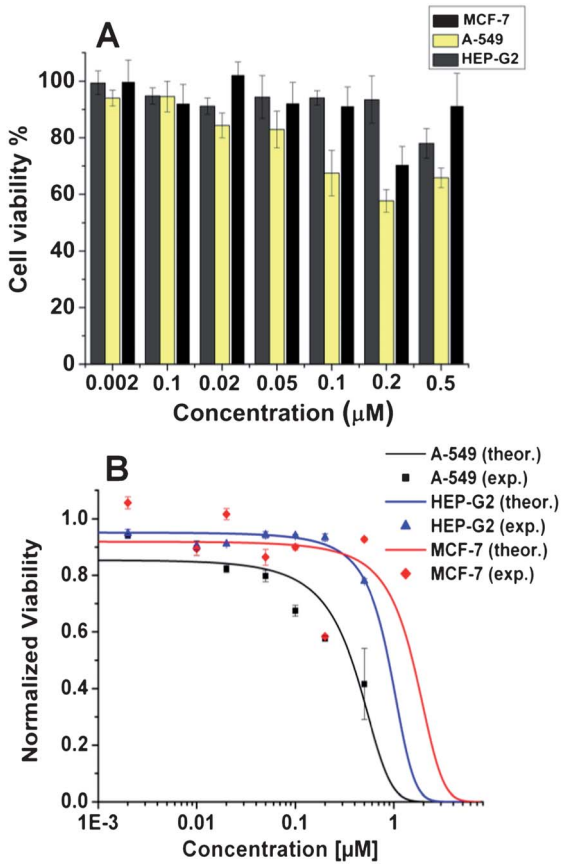

Fig. 5 The effect of P14/QDs concentration on the survival of MCF-7, A-549 and HEP-G2 cells treated with P14/QDs conjugates at 0.002, 0.01, 0.02, 0.05, 0.1, 0.2 and 0.5 μM for 4 h. A) Cell viability results evaluated *via* MTT assay, B) dose–response curves extrapolated from MTT data. After 4 h of treatment with P14/QDs conjugates at concentrations higher than 0.1 μM, decrease in cell viability was observed for A-549 cells. However, in the case of MCF-7 and HEP-G2 cells, conjugates up to 0.5 μM didn't cause any significant toxic effect. Values are the mean ± standard deviation of the data ($N = 4$).

QDs are dispersed in toluene, the MTT test couldn't be performed with native QDs because toluene elicited very high toxicity to the cells (data not shown). It has been found that QDs with a stable polymer coating such as PAMAM are essentially nontoxic to the MCF-7 and HEP-G2 cells. Thus, it can be claimed that toxicity does not arise from even PAMAM molecules on QD surface. However, they have an effect on cellular ATP production or cell replication of A-549 at the QDs concentration higher than 0.1 μM.

Cytotoxicity data obtained from the MTT assay was extrapolated using exponential regression analysis which was based on an equation derived from the exponential equation ($y = 1 - \frac{1}{1 + e^{a(b-x)}}$), where a is the curve slope, b is IC_{50} (50% inhibitory concentration) and x is the concentration of sample (Fig. 5B). IC_{50} was determined automatically while calculating the equation. Also, NOAEC (no observable adverse effect concentration) and TLC (total lethal concentration) were determined using similar equations. Estimated toxicity values in terms of IC_{50}, NOAEC and TLC are displayed in Table 1. According to the results, P/QDs conjugates are more toxic for A-549 (IC_{50} 0.373 μM) cells than MCF-7 (IC_{50} 1.549 μM) and HEP-G2 cells (IC_{50} 0.885 μM).

In vitro studies

When QDs are coupled with biological molecules such as receptor ligands, specific uptake occurs *via* receptor-mediated endocytosis. Besides specific binding, transport across cellular membranes can be achieved with non-specific binding of polycationic ligands as well. Amine-terminated dendrimers are reported to bind to cells in a non-specific manner owing to positive charge.[43] By partial acetylation of surface amine groups of PAMAM[43–46] or adding biocompatible polymers such as PEG,[47] some studies tried to cope with this problem. Herein possible non-specific interactions as a function of ligand density and surface charge were examined by treating MCF-7 cells with QDs conjugates derivatized with two different amounts of PAMAM molecules (14 and 28 molecules). Fluorescence images of the cells are represented in Fig. 6. Obviously, P28/QDs conjugates were attached to the cell surface much more effectively than P14/QDs conjugates could attach. Thus, it can be claimed that P14/QDs conjugates potentially have negligible interactions with cell surfaces.

For *in vitro* cellular uptake experiments, P14/QDs conjugates have been utilized in targeting a breast cancer cell line (MCF-7) by coupling the HER2 receptor specific antibody to the P/QDs conjugates. Covalent attachment of the antibody to P14/QDs conjugates was achieved by applying a EDC/NHS cross-linking reaction. It has been reported that HER2-overexpressing cells internalize targeted molecules *via* HER2 receptor-mediated endocytosis.[46,48] Fluorescence microscopy images of MCF-7 cells labelled with P/QDs-AntiHER2 conjugates at 0.9 and 0.5 μM QDs concentrations are shown in Fig. 7. It can be seen that conjugates with 0.9 μM QDs were totally spread out in the cytosol (Fig. 7A) whereas P/QDs-AntiHER2 with a lower concentration (0.5 μM) of QDs (Fig. 7B) stayed on the outer membrane after 4 h of incubation. In order to check if the internalization process is driven by endocytotic pathways, MCF-7 cells were incubated with P/QDs-AntiHER2 conjugates and P/QDs conjugates at 4 °C. According to the fluorescence images illustrated in Fig. 8, it is apparent that HER2 specific antibody labelled P/QDs conjugates are taken up into the cell *via* endocytotic pathways.

Discussion

The ligand-exchange reaction between PAMAM and QDs is based on the strong binding affinity of multiple amine groups to

Table 1 Calculated cytotoxicity values for P14/QDs conjugates using MTT assay. Cytotoxicity results based on cell viability data were expressed as no observable adverse effect concentration (NOAEC), 50% inhibitory concentration (IC_{50}) and total lethal concentration (TLC) values (μM). P14/QDs conjugates have toxic influence on cell proliferation at A-549 cells with IC_{50} 0.373 μM

Cell lines	IC_{50} (μM)	NOAEC (μM)	TLC (μM)
MCF-7	1.549	0.320	3.427
A-549	0.373	0.065	0.996
HEP-G2	0.885	0.218	1.762

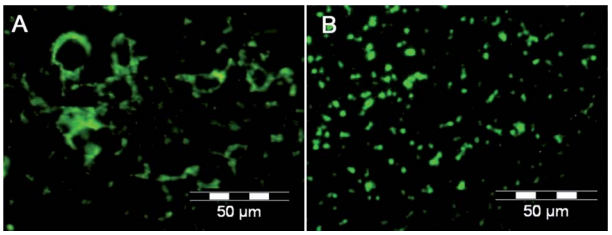

Fig. 6 Fluorescence microscopy images of MCF-7 cells treated with (A) QDs nanocrystals modified with *ca.* 28.0 PAMAM dendrimers, and (B) QDs nanocrystals modified with *ca.* 14.1 PAMAM dendrimers for 4 h. Possible non-specific interactions of P/QDs conjugates with cells were examined as a function of density of surface groups. QDs with 28 PAMAM molecules interact with cell surface much more intensively *via* electrostatic interactions compared to QDs with 14 PAMAM molecules.

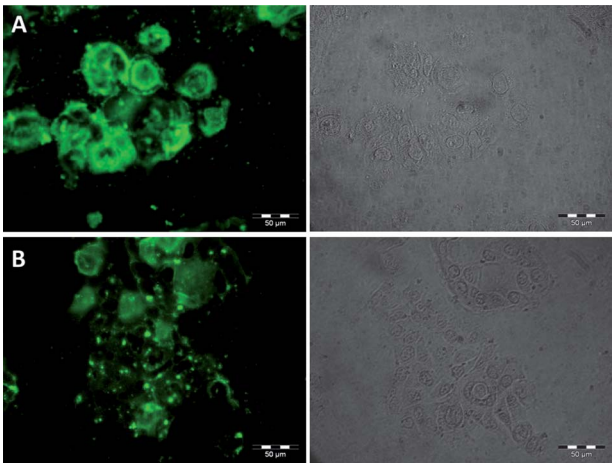

Fig. 7 Cellular uptake of P/QDs-AntiHER2 conjugates. (A) MCF-7 cell treated with Anti-HER2 coupled P/QDs conjugates at 0.9 μM QDs concentration, and (B) with 0.5 μM QDs concentration. Right panel shows the bright field images of cells, and the left panel shows the QDs fluorescence at 563 nm. Cells are observed under fluorescence microscopy after 4 h of incubation at 37 °C.

zinc atoms on the QD surface. It has been found that it is essential to use the same coordinating groups for the exchange reaction; that is, one primary amine group in the original capping ligand is exchanged with another primary amine group in the multivalent ligand. This strategy allows the creation of more stable polymer-derivatized QDs.[47] QDs originally stabilized with a mixture of TOPO/HDA were also exposed to the same ligand-exchange reaction with PAMAM. However, aggregates formed, showing the inefficient ligand-exchange reaction between TOPO and PAMAM and uncontrolled adsorption of dendrimers to the QDs surfaces. This also proves that when the ligand-exchange reaction is carried out between the same functional groups, the efficiency of the surface modification process becomes much better. On the other hand, it is worth mentioning that giving QDs a hydrophilic surface consisting of PAMAM molecules decreases the fluorescence of quantum dots. That is to say, the fluorescence efficiency of hydrophobic QDs is much higher in organic solvents than that of hydrophilic QDs in aqueous solutions.[38] Although, they do retain their basic optical properties such as the absorption and emission spectrum profiles (Fig. 2). Furthermore, the

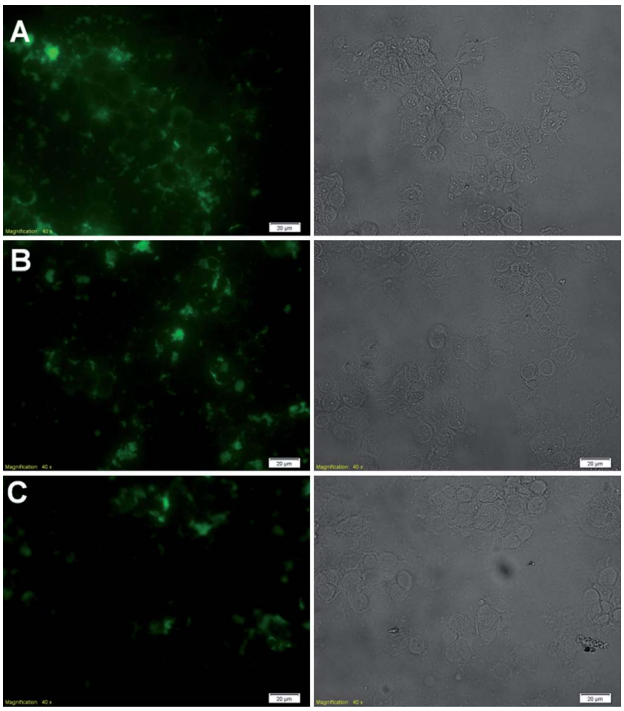

Fig. 8 Evaluation of MCF-7 cells incubated with (A) Anti-HER2 coupled P/QDs conjugates at 0.9 μM QDs concentration, (B) with 0.5 μM QDs concentration, and (C) 0.5 μM P/QDs conjugates. Right panel shows the bright field images of cells, and the left panel shows the QDs fluorescence at 563 nm. Cells are observed under fluorescence microscopy after 4 h of incubation at 4 °C.

remaining fluorescence signal is strong enough to label the cells and evaluate them under fluorescence microscopy due to the reduced photobleaching effect of QDs.

When QDs were modified with different amounts of PAMAM as illustrated in Fig. 3, it was found out that the QD surface is covered with a maximum of 28 PAMAM molecules with a coupling yield of 93.3%. Concomitant increasing fluorescence intensities imply that the increase in ratio of PAMAM results in an increase of QD nanoparticles solubilized in water through phase-transfer reactions. When the QD surface was totally covered with PAMAM, fluorescence of conjugates reached a steady state which means no more QDs pass through the water phase. The coverage of QDs should be dictated by steric effects. However these steric effects are likely balanced by interchain interactions arising from the intervoid structure of PAMAM, which may form densely packed structures on the QD surface. Thus, the QD surface reaches a maximum binding point by virtue of these restoring interactions.

In the case of surface processing of QDs *via* ligand-exchange reactions, it is very challenging to obtain controllable ligand ratios on the QD surface with high coupling efficiencies. Apparently, efficient phase-transfer reaction of QDs was accomplished, which is attributed to the electrostatic stabilizing feature of multiple positive groups of PAMAM dendrimers. It is important to mention that the ligand-exchange reaction is based on the binding affinity of amines to Zn atoms, which causes solubilization of QDs. Zinc atoms and amines are hard acid and hard bases, respectively. It is well known that hard acid–hard

base interactions are stronger than hard acid–soft base interactions. Thus, strong binding affinity may exhibit a leading role in stabilization of QDs, along with electrostatic interactions. Since PAMAM has interior void structures,[22] there might be intermolecular interactions between PAMAM molecules on the QDs surface. In other words, PAMAM molecules could interact with neighboring PAMAM molecules. Further, these interactions can be supported by hydrogen bond networking which is formed by terminal amine groups of PAMAM.[30] Dendrimer chains with steric crowding characteristics may also allow closely packed structure on the QDs surface which results in improved fluorescence efficiency.[32] As a consequence, these anticipated mechanisms may form packed densely PAMAM molecules on QD surface which in turn promote structural stabilization. Evidently, it can be asserted that the surface manipulating strategy that was applied to QD allowed us to create QD probes with better understandable structural properties which control or determine future aspects of QDs.

The issue of cell responses to a variety of nanoparticles may be specified by cell surface morphology, cell specific surface receptors and their characteristic distribution in those cells. It can be claimed that the different surface morphology of A-549 cells makes the cells more susceptible to the cytotoxic effects of P/QDs than that of MCF-7 and HEP-G2 cell lines (Fig. 5). This assumption is supported by a study of Patra *et al.* that reported gold nanoparticles (GNP) induce cell death response in A-549 cells. On the other hand, the two other cell lines tested, BHK21 (baby hamster kidney) and HEP-G2, remained unaffected by GNP treatment.[49] Moreover, Choi *et al.* demonstrated that PEG-derivatized phospholipid coated Fe_3O_4 and MnO metal oxide nanoparticles elicited a more toxic effect for A-549 cells than that of MCF-7 cells according to live/death cell and LDH assay kit after 2 h of incubation.[50] Although obtained results for *in vitro* cytotoxic effect of P/QDs conjugates were promising, the transferability of the data to *in vivo* experiments is not clear yet.

In the cell culture experiments, a striking difference was observed between the cells treated with P14/QDs and P28/QDs conjugates (Fig. 6). Cells became distinguishable when they were stained with P28/QDs conjugates due to the higher density of dendrimer molecules, and therefore a higher density of surface positive charges, on the QD surface. On the other hand, lower ligand density on the QD surface weakened the electrostatic interactions of P14/QDs conjugates with the cell surface, which were not strong enough to visualize the cells. Hence, P/QDs conjugates containing 14.1 ± 0.46 PAMAM molecules were used for antibody coupling and further cell targeting experiments due to their reduced size and reduced non-specific interactions in order to improve specific targeting efficiency.

As mentioned before, cationic polymers have a strong pH-buffering capacity. In acidic organelles this enhances proton adsorption and builds up osmotic pressure across the cell membrane. This process in turn promotes the endosomal escape and release of the polymer to the cytosol.[28,47] QDs are trapped in endosomes/lysosomes after internalization, resulting in the irreversible destruction of photochemical fluorescence of QDs, caused by a pH value of around 4.0–5.0.[29,51,52] In order to utilize QDs for cellular targeting and drug delivery studies, these disadvantages should be overcome. Surface derivatization of QDs with PAMAM, which possesses strong buffering capacity, is expected to accelerate endosomal escape, which prevents photobleaching of QDs. This enhances cytoplasmic migration of QDs in cells and at the same time increases the photostability of QDs during long-term treatments. Fluorescence microscopy images demonstrate effective attachment and cellular internalization of the HER2 receptor specific antibody targeted P/QDs conjugates (Fig. 7). Combination of the conjugates with an antibody represents a potentially viable method with better specificity and enhanced cellular targeting efficiency in comparison to that of label free P/QDs conjugates. After 4 h of incubation, P/QDs-AntiHER2 bioconjugates not only bound to outer surface but also internalized into the cells whereas P14/QDs conjugates could only interact inefficiently with the cell surface in a non-specific manner (Fig. 6B). As a result, it was proved that structurally stabilized bioconjugates with the enhanced photo-brightness of QDs, the strong buffering capacity of PAMAM, and the presence of a targeting moiety lead to efficient *in vitro* labelling and imaging of tumor cells.

Conclusions

Researches in quantum dot (QD) probe design and development have focused on synthesis, solubilization and coupling of QDs with target-specific ligands. Several strategies are being used to manipulate surface ligands as well as their molar ratios with respect to QDs. However, the 'best' QD probes with controlled ligand molar ratios aren't available yet. Herein, we described surface processing of quantum dots (QDs) with amine-terminated polyamidoamine (PAMAM) dendrimers with controllable molar ratios of PAMAM. We conclude that PAMAM dendrimers with amino moieties are found to solubilize QDs in aqueous solvents through ligand-exchange reactions. It was found that ligand density on the QD surface has a major effect on possible non-specific interactions with cell surfaces. The most challenging aspects of the use of amine groups are their concentration-dependent toxic effects and their non-specific interactions with cell surfaces. When we switched to cell culture experiments, we tried to eliminate those foreseen undesired interactions by manipulating the ligand density on the QD surface. As a result, a large part of the non-specific interactions were eliminated. Fluorescence microscopy images of cells stained with antibody coupled P/QDs conjugates proved that non-specific interactions are reduced regardless. These extracted results will suggest better surface processing strategies to take one step towards finding the 'best' QD nanocomplexes. The *in vitro* application studies presented above show that PAMAM-derivatized QDs conjugates targeted with HER2 receptor specific antibodies are capable of labelling cancer cells in a specific manner. It should be emphasized that well characterized P/QDs conjugates allowed us to build up engineered devices with up-and-coming features for cell targeting and imaging experiments.

Although the cited studies have promising points, further studies should focus on detailed physical parameters such as surface charge and colloidal stability which determine QDs ability to interact with cell surface, be endocytosed, escape from endosomes, and/or enter the nucleus, and biological interactions for different cells/processes.[53] The results presented in this study will suggest important guidelines to highlight some of these

concerns in order to design multifunctional dendrimer based quantum dots as fluorescent probes for cellular imaging.

Materials and methods

Chemicals

PAMAM dendrimer (P-G5; ethylenediamine core, generation 5.0 solution), ethyl acetate (≥99.8%), tetramethylammonium hydroxide solution (25 wt% in methanol), *N*-(3-dimethylaminopropyl)-*N*′-ethylcarbodiimide hydrochloride (EDC), *N*-hydroxysuccinimide (NHS) and CdSe/ZnS (560 nm, 5 mg mL^{-1} in toluene, HDA ligand coated, 694630) were purchased from Sigma-Aldrich. Phosphate buffer saline (PBS) was prepared with 8.01 g L^{-1} sodium chloride, 0.2 g L^{-1} potassium chloride, 1.44 g L^{-1} disodium hydrogen phosphate and 0.24 g L^{-1} potassium dihydrogen phosphate, pH 7.4. Anti-HER2 (c-erbB-2) Clone TAB250 as well as Minimum Essential Medium powder (MEM) were obtained from Invitrogen. Dulbecco's Modified Eagle's Medium powder-high glucose (DMEM), human insulin solution and 3-(4,5-dimethylthiazol-2-yl)-2,5-diphenyl tetrazolium bromide (MTT) were purchased from Sigma-Aldrich. Sodium dodecyl sulfate (SDS) was provided by Applichem. All other medium ingredients were purchased from PAA Laboratories GmbH. The applied human cancer cell lines MCF-7 (breast cancer), A-549 (lung cancer), HEP-G2 (liver cancer) were ordered from DSMZ (German Collection of Microorganisms and Cell Cultures).

Synthesis of water soluble P/QDs conjugates

0.5 mL of CdSe/ZnS core-shell QDs in toluene solution (5.0 μM), 0.5 mL of the PAMAM G5 dendrimer in methanol solution (150 μM) and 50 μL tetramethylammonium hydroxide solution were added to a vial. The mixture was shaken for 15 h at 30 °C. Then 2.0 mL ethyl acetate was added to the vial to precipitate the nanocrystal complexes. The solution was centrifuged and the purified PAMAM coated CdSe/ZnS QDs were dissolved in PBS buffer solution. Unconjugated PAMAM dendrimers were separated *via* filtration with 50 kDa MWCO centrifugal membrane tubes (Millipore Amicon Ultra 0.5 mL, USA). The number of coupled PAMAM molecules was estimated by using Bradford reactive.

Conjugation of Anti-HER2 antibody to P/QDs conjugates (P/QDs-AntiHER2)

To activate the carboxyl-terminus of the antibody, 0.1 M EDC and 0.25 M NHS solutions in 25.0 mM pH 6.0 MES buffer were added to Anti-HER2 antibodies (0.01 mg mL^{-1}). After 15 minutes constant shaking at room temperature, aqueous solution of P/QDs at 5.0 μM QDs concentration in pH 7.4 PBS buffer was added. The solution was stirred for 2 hours at room temperature for antibody conjugation. Unconjugated antibodies, P/QDs and excess EDC and NHS were removed by centrifugation with 300 kDa MWCO membrane filtration tubes (VWR Nanosep Omega, Germany).

Fluorescence measurements

Fluorescence spectra of QDs conjugates were measured by using 2.0 μL of sample with a Nanodrop 3300 spectrofluorometer (Thermo Fisher Scientific Inc. USA) in terms of relative fluorescence units (RFU). The effect of conjugation on the fluorescence characteristics of QDs nanoparticles was examined according to the fluorescence spectrum. Also absorbance of conjugates was measured with a NanoDrop 1000 spectrophotometer (Thermo Fisher Scientific Inc. USA).

Size characterization

The hydrodynamic diameters of P/QDs conjugates dissolved in PBS pH 7.4 were evaluated by using dynamic light scattering (DLS). DLS data were collected by using a Malvern DLS apparatus (Nano-ZS) with a 633 nm He/Ne laser. JSM 6700F NT model SEM (Scanning Electron Microscopy) was also used to evaluate the size of the P/QDs conjugates.

Cell culture experiments

MCF-7 cell line was grown in Minimum Essential Medium Eagle (MEM) modified with 10% fetal calf serum, 1.0 mM sodium pyruvate, 2.0 mM L-glutamine, 10 μg mL^{-1} insulin, 1.0% non-essential amino acids and 10 mL L^{-1} penicillin/streptomycin. A-549 and HEP-G2 cell lines were grown in Dulbecco's Modified Eagle Medium (DMEM) containing 10% fetal calf serum and 1% penicillin/streptomycin. Cells were cultured at 37 °C in a moist atmosphere containing 5.0% CO_2. For incubation of the cells with samples or during cytotoxicity tests the same conditions were used.

In vitro cytotoxicity

Dose dependent cytotoxicity effects of P/QDs were evaluated by using standard 3-(4,5-dimethylthiazol-2-yl)-2,5-diphenyl tetrazolium bromide (MTT) assays. Briefly, in 96-well flat bottom tissue plates abundantly populated MCF-7 and typical model cell lines, A-549 and HEP-G2, were treated with P/QDs conjugates at 0.5, 0.2, 0.1, 0.05, 0.02, 0.01 and 0.002 μM QDs concentrations for 4 h. Then the samples were removed completely to avoid any reactions of MTT with reducing components of the medium or sample. To work out the cytotoxic effects of the different P/QDs concentrations, cells were incubated with 110 μL/well MTT solution (10%, 5.0 mg mL^{-1} PBS) in medium for 4 h. Living cells with metabolic activity are able to reduce the yellow MTT to a purple-colored formazan complex inside the cells. Then 100 μL SDS (1.0 g SDS in 10 mL 0.01 M HCl) was applied to the wells to dissolve the purple crystals. After 24 h of incubation, UV-Vis absorption was measured at 570 nm with 630 nm as reference wavelength. Therefore, a microplate reader Model 680 (BioRad) was used.

Fluorescence microscopy

Fluorescence microscopy images were captured with an Olympus IX50 (Olympus America Inc.) fluorescence microscope equipped with a digital camera (Olympus, C3040-ADU, Japan). The images were processed with Cell^B image analysis software (Olympus, Japan). For monitoring fluorescence labelled cells, excitation filter U-MNB (filter), DM500 (dichroic mirror), BP470-490 (exciter filter), BA515 (barrier filter) were used. Before labelling MCF-7 cells with P/QDs-AntiHER2 conjugates,

the cells were seeded out in 96-well flat bottom tissue plates. After 3 days of cultivation, wells were populated abundantly, old culture medium was discarded and cells were washed twice with PBS. Afterwards, cells were treated with 100 μL of conjugate diluted with medium, and incubated for 4 h at 37 °C. Finally, cells were rinsed twice with PBS to remove excess conjugate.

Acknowledgements

This work is granted by Scientific and Technological Research Council of Turkey (TUBITAK, project number 109T573) and Federal Ministry of Education and Research (BMBF, project number TUR 09/125). Also it was partially funded by Ege University Scientific Research Project (2010/FEN/0053) and Ege University Science-Technology Research and Application Center (2010BIL004). We are grateful to M.Sc. Stefanie Wagner (Gottfried Wilhelm Leibniz University of Hannover, Institute for Technical Chemistry) for providing valuable advice about MTT analysis. In addition, we thank M.Sc. Clarissa Baumanis (Gottfried Wilhelm Leibniz University of Hannover, Institute for Technical Chemistry) for operating SEM analysis. Finally we appreciate Dr Ilker Medine (Ege University, Institute of Nuclear Sciences) for technical support in cell culture experiments.

Notes and references

1 M. Dahan, T. Laurence, F. Pinaud, D. S. Chemla, A. P. Alivisatos, M. Sauer and S. Weiss, *Opt. Lett.*, 2001, **26**, 825–827.
2 X. H. Gao, Y. Y. Cui, R. M. Levenson, L. W. K. Chung and S. M. Nie, *Nat. Biotechnol.*, 2004, **22**, 969–976.
3 S. S. Feng and J. Pan, *Biomaterials*, 2009, **30**, 1176–1183.
4 C. Chen, J. Peng, H. S. Xia, G. F. Yang, Q. S. Wu, L. D. Chen, L. B. Zeng, Z. L. Zhang, D. W. Pang and Y. Li, *Biomaterials*, 2009, **30**, 2912–2918.
5 C. M. Lee, D. Jang, S. J. Cheong, E. M. Kim, M. H. Jeong, S. H. Kim, D. W. Kim, S. T. Lim, M. H. Sohn and H. J. Jeong, *Nanotechnology*, 2010, **21**, 285102.
6 L. Yang, H. Mao, Y. A. Wang, Z. Cao, X. Peng, X. Wang, H. Duan, C. Ni, Q. Yuan, G. Adams, M. Q. Smith, W. C. Wood, X. Gao and S. Nie, *Small*, 2009, **5**, 235–243.
7 K. T. Yong, H. Ding, I. Roy, W. C. Law, E. J. Bergey, A. Maitra and P. N. Prasad, *ACS Nano*, 2009, **3**, 502–510.
8 B. R. Liu, Y. W. Huang, J. G. Winiarz, H. J. Chiang and H. J. Lee, *Biomaterials*, 2011, **32**, 3520–3537.
9 R. Bakalova, Z. Zhelev, I. Aoki, K. Masamoto, M. Mileva, T. Obata, M. Higuchi, V. Gadjeva and I. Kanno, *Bioconjugate Chem.*, 2008, **19**, 1135–1142.
10 K. C. Weng, C. O. Noble, B. Papahadjopoulos-Sternberg, F. F. Chen, D. C. Drummond, D. B. Kirpotin, D. Wang, Y. K. Hom, B. Hann and J. W. Park, *Nano Lett.*, 2008, **8**, 2851–2857.
11 B. B. Atmaja, B. H. Lui, Y. Hu, S. E. Beck, C. W. Frank and J. R. Cochran, *Adv. Funct. Mater.*, 2010, **20**, 4091–4097.
12 Y. He, Y. Zhong, Y. Su, Y. Lu, Z. Jiang, F. Peng, T. Xu, S. Su, Q. Huang, C. Fan and S. T. Lee, *Angew. Chem., Int. Ed.*, 2011, **50**, 5695–5698.
13 V. Biju, S. Mundayoor, R. V. Omkumar, A. Anas and M. Ishikawa, *Biotechnol. Adv.*, 2010, **28**, 199–213.
14 N. Chaniotakis and M. F. Frasco, *Anal. Bioanal. Chem.*, 2010, **396**, 229–240.
15 I. L. Medintz, H. T. Uyeda, E. R. Goldman and H. Mattoussi, *Nat. Mater.*, 2005, **4**, 435–446.
16 A. M. Smith, H. Duan, A. M. Mohs and S. Nie, *Adv. Drug Delivery Rev.*, 2008, **60**, 1226–1240.
17 T. Jamieson, R. Bakhshi, D. Petrova, R. Pocock, M. Imani and A. M. Seifalian, *Biomaterials*, 2007, **28**, 4717–4732.
18 V. Biju, T. Itoh and M. Ishikawa, *Chem. Soc. Rev.*, 2010, **39**, 3031–3056.
19 S. M. Nie and W. C. W. Chan, *Science*, 1998, **281**, 2016–2018.
20 W. J. Parak, T. Pellegrino and C. Plank, *Nanotechnology*, 2005, **16**, R9–R25.
21 T. Jin, D. K. Tiwari, S. I. Tanaka, Y. Inouye, K. Yoshizawa and T. M. Watanabe, *Sensors*, 2009, **9**, 9332–9354.
22 D. A. Tomalia, A. R. Menjoge and R. M. Kannan, *Drug Discovery Today*, 2010, **15**, 171–185.
23 A. S. Chauhan, N. K. Jain, P. V. Diwan and A. J. Khopade, *J. Drug Targeting*, 2004, **12**, 575–583.
24 J. Khandare, P. Kolhe, O. Pillai, S. Kannan, M. Lieh-Lai and R. M. Kannan, *Bioconjugate Chem.*, 2005, **16**, 1049–1049.
25 O. Boussif, F. Lezoualch, M. A. Zanta, M. D. Mergny, D. Scherman, B. Demeneix and J. P. Behr, *Proc. Natl. Acad. Sci. U. S. A.*, 1995, **92**, 7297–7301.
26 A. S. Verkman, N. D. Sonawane and F. C. Szoka, *J. Biol. Chem.*, 2003, **278**, 44826–44831.
27 Y. Higuchi, C. Wu, K. L. Chang, K. Irie, S. Kawakami, F. Yamashita and M. Hashida, *Biomaterials*, 2011, **32**, 6676–6682.
28 R. Langer, A. Akinc, M. Thomas and A. M. Klibanov, *Journal of Gene Medicine*, 2005, **7**, 657–663.
29 J. Silver and W. Ou, *Nano Lett.*, 2005, **5**, 1445–1449.
30 L. S. Santos, D. A. Geraldo, E. F. Duran-Lara, D. Aguayo, R. E. Cachau, J. Tapia, R. Esparza, M. J. Yacaman and F. D. Gonzalez-Nilo, *Anal. Bioanal. Chem.*, 2011, **400**, 483–492.
31 D. A. Tomalia and B. H. Huang, *J. Lumin.*, 2005, **111**, 215–223.
32 X. G. Peng, Y. A. Wang, J. J. Li and H. Y. Chen, *J. Am. Chem. Soc.*, 2002, **124**, 2293–2298.
33 Q. S. Ren, Z. M. Li, P. Huang, R. He, J. Lin, S. Yang, X. J. Zhang and D. X. Cui, *Mater. Lett.*, 2010, **64**, 375–378.
34 Y. Zhao, S. Liu, Y. Li, W. Jiang, Y. Chang, S. Pan, X. Fang, Y. A. Wang and J. Wang, *J. Colloid Interface Sci.*, 2010, **350**, 44–50.
35 M. M. Bradford, *Anal. Biochem.*, 1976, **72**, 248–254.
36 W. B. Cai, D. W. Shin, K. Chen, O. Gheysens, Q. Z. Cao, S. X. Wang, S. S. Gambhir and X. Y. Chen, *Nano Lett.*, 2006, **6**, 669–676.
37 M. Dahan, S. Levi, C. Luccardini, P. Rostaing, B. Riveau and A. Triller, *Science*, 2003, **302**, 442–445.
38 T. Nann, *Chem. Commun.*, 2005, 1735–1736.
39 A. Hoshino, K. Fujioka, T. Oku, M. Suga, Y. F. Sasaki, T. Ohta, M. Yasuhara, K. Suzuki and K. Yamamoto, *Nano Lett.*, 2004, **4**, 2163–2169.
40 A. M. Derfus, W. C. W. Chan and S. N. Bhatia, *Nano Lett.*, 2004, **4**, 11–18.
41 D. Fischer, Y. Li, B. Ahlemeyer, J. Krieglstein and T. Kissel, *Biomaterials*, 2003, **24**, 1121–1131.
42 R. Jevprasesphant, J. Penny, R. Jalal, D. Attwood, N. B. McKeown and A. D'Emanuele, *Int. J. Pharm.*, 2003, **252**, 263–266.
43 R. Shukla, T. P. Thomas, J. Peters, A. Kotlyar, A. Myc and J. R. Baker, Jr., *Chem. Commun.*, 2005, 5739–5741.
44 I. J. Majoros, T. P. Thomas, C. B. Mehta and J. R. Baker, Jr., *J. Med. Chem.*, 2005, **48**, 5892–5899.
45 I. J. Majoros, A. Myc, T. Thomas, C. B. Mehta and J. R. Baker, Jr., *Biomacromolecules*, 2006, **7**, 572–579.
46 R. Shukla, T. P. Thomas, J. L. Peters, A. M. Desai, J. Kukowska-Latallo, A. K. Patri, A. Kotlyar and J. R. Baker, Jr., *Bioconjugate Chem.*, 2006, **17**, 1109–1115.
47 H. Duan and S. Nie, *J. Am. Chem. Soc.*, 2007, **129**, 3333–3338.
48 K. Langer, H. Wartlick, K. Michaelis, S. Balthasar, K. Strebhardt and J. Kreuter, *J. Drug Targeting*, 2004, **12**, 461–471.
49 H. K. Patra, S. Banerjee, U. Chaudhuri, P. Lahiri and A. K. Dasgupta, *Nanomed.: Nanotechnol., Biol. Med.*, 2007, **3**, 111–119.
50 J. Y. Choi, S. H. Lee, H. Bin Na, K. An, T. Hyeon and T. S. Seo, *Bioprocess Biosyst. Eng.*, 2010, **33**, 21–30.
51 Y. H. Sun, Y. S. Liu, P. T. Vernier, C. H. Liang, S. Y. Chong, L. Marcu and M. A. Gundersen, *Nanotechnology*, 2006, **17**, 4469–4476.
52 N. Tamai and A. Mandal, *J. Phys. Chem. C*, 2008, **112**, 8244–8250.
53 J. L. Nadeau, S. J. Clarke, C. A. Hollmann and F. A. Aldaye, *Bioconjugate Chem.*, 2008, **19**, 562–568.

